Improving salt boundary imaging using an RTM inverse scattering imaging condition

Sang Suh and Bin Wang, TGS

SUMMARY

Reverse time migration (RTM) suffers from low wavenumber noise especially above strong reflectors such as salt boundaries. The traditional method of removing the noise is applying low cut filtering, which could destroy real events. The inverse scattering imaging condition selectively removes the backscattering noise. We introduce a method of computing the inverse scattering weighting coefficient. Synthetic and field examples show that the inverse scattering imaging improves salt boundary imaging compared to post-processed conventional RTM. The complicated imaging algorithm requires more computing time. The main overhead comes from the increased amount of source wavefield data. By redistributing some of the data compression process to the GPU's, we were able to reduce the run time overhead by 10% of the conventional RTM.

INTRODUCTION

Reverse time migration (RTM) computes subsurface images by cross-correlating source and receiver wavefields (Claerbout, 1971). However, RTM images suffers from low wavenumber noise due to the unwanted cross-correlation of head waves, diving waves, and backscattered waves. Various methods have been proposed to suppress the RTM noise. Mulder and Plessix (2003) proposed a low cut filtering in the space domain. Chang and McMechan (1986, 1990) suggested ray-traced imaging condition, in which source wavefield after the first arrival is limited to some fixed time duration. Fletcher et al. (2006) used modified wave equation to include the damping term in areas of the velocity model where strong unwanted reflections are created.

Another method of removing the RTM noise is wavefield separation. Yoon and Marfurt (2006) introduced the Poynting vector which will determine the direction of wave propagation and to decompose into upgoing and downgoing waves. Liu et al. (2007) decomposed the full wavefield into its one-way components, and applied the imaging condition to the appropriate combinations of the wavefield components. Suh and Cai (2009) used a fan filtering plus wavefield decomposition method. Yan and Xie (2009) prposed an angle-domain imaging condition by decomposing the full wavefields at every image location to local plane waves of different directions.

Kaelin and Carvajal (2011) introduced time-shift imaging condition. Xie et al. (2012) applied a similar approach, called Delayed Imaging Time (DIT) gathers to enhance the top-of-salt RTM images.

Whitmore and Crawley (2012) introduced an inverse scattering imaging condition. The method creates two separate images: a gradient image and a time derivative image. These two images are weighted summed using a weighting function to produce the backscattering free RTM image. This method is very attractive both in terms of implementation and image quality.

In this abstract we review the RTM inverse scattering imaging condition and introduce a method of computing the position dependent weighting coefficients. We present synthetic and field data examples. Also, we discuss the run time overhead of this new imaging condition compared to the conventional cross-correlation RTM imaging method.

METHOD

Acccording to Whitmore and Crawley (2012), the RTM inverse scattering image is given by

$$I(\mathbf{x}) = \frac{1}{W(\mathbf{x})}\left[I_\nabla(\mathbf{x}) + B(\mathbf{x})I_{dt}(\mathbf{x})\right] \tag{1}$$

where $W(\mathbf{x})$ is an approximate amplitude correction which could include source power, transmission effects, etc. $B(\mathbf{x})$ is the weighting coefficient to attenuate the backscattered energy. Here, $I_\nabla(\mathbf{x})$ and $I_{dt}(\mathbf{x})$ are defined by

$$I_\nabla(\mathbf{x}) = \int \nabla\psi_s(\mathbf{x},t)\cdot\nabla\psi_r(\mathbf{x},T-t)\,dt \tag{2}$$

$$I_{dt}(\mathbf{x}) = \frac{1}{V^2(\mathbf{x})}\int \frac{\partial}{\partial t}\psi_s(\mathbf{x},t)\frac{\partial}{\partial t}\psi_r(\mathbf{x},T-t)\,dt \tag{3}$$

where ψ_s and ψ_r are the source and receiver wavefields scaled by $\omega^{-\alpha}$ with α being chosen to compensate the frequency modulation effect of the gradient and time derivative operations. We call $I_\nabla(\mathbf{x})$, the gradient image, and $I_{dt}(\mathbf{x})$, the time derivative image.

Our method of computing the weighting coefficient is as follows. In Equation 1, $B(\mathbf{x})$ acts as the weighting coefficient to attenuate the backscattered wave, turning wave, and wide reflection energies. Because RTM back scattering noise appears as a low wavenumber event, the appropriate weighting is a smooth function of the position $\mathbf{x}$, and can be computed by

$$B(\mathbf{x}) = \min\left[B_{max}, \max\left(B_{min}, \frac{\tilde{I}_\nabla(\mathbf{x})}{\tilde{I}_{dt}(\mathbf{x})}\right)\right], \tag{4}$$

where $\tilde{I}_\nabla$ and $\tilde{I}_{dt}$ are high-cut filtered versions of the corresponding wavefields. Here B_{min} and B_{max} are minimum and maximum values of $B(\mathbf{x})$.

Conventional post-RTM low-cut filtering is equivalent to the unconstrained weighting coefficient,

$$\hat{B}(\mathbf{x}) = \frac{\tilde{I}_\nabla(\mathbf{x})}{\tilde{I}_{dt}(\mathbf{x})} \tag{5}$$

because it is designed to remove low wavenumber components which may destroy real events having long wavelengths.

The high-cut filtered wavefields, $\tilde{I}_\nabla$ and $\tilde{I}_{dt}$ can be created by applying a simple band-pass filter with cut-off beginning at

DOI http://dx.doi.org/10.1190/segam2013-0686.1

wavenumber, k_1, and cut-off ending at wavenumber, k_2, expressed in radial wavenumbers. The radial wavenumber, k, is defined by

$$k = \sqrt{k_x^2 + k_y^2 + k_z^2}, \tag{6}$$

where k_x, k_y, and k_z are the wavenumbers in x-, y-, and z-axis respectively.

Figure 1 shows the inverse scattering imaging process. Figure 1a is the gradient image, I_∇. Figure 1b is the time derivative image, I_{dt}. Figure 1c is the weighting coefficient, $B(\mathbf{x})$, in Equation 4. Figure 1d is the inverse scattering RTM image, i.e., the weighted sum of (a) and (b).

EXAMPLES

Figure 2 compares the post-processed conventional RTM and inverse scattering RTM. The input is BP 2004 synthetic model (Billette et al., 2005). Conventional RTM image is created using a 25m grid interval, 20 Hz maximum frequency, and 12,000 m half-aperture width. The migrated image was low-cut filtered and is shown in Figure 2a. The low cut filter cut-off parameters are $k_1 = 0.12k_{max}$, and $k_2 = 0.18k_{max}$, respectively. Figure 2b is the inverse scattering RTM image, using the computational parameters as in Figure 1.

Figure 3 shows zoomed views of the left and right salt bodies of Figure 2. The figures demonstrate that the salt boundary is better imaged by inverse scattering RTM than by post-processed conventional RTM.

Figure 4 shows a zoomed view comparing the images for the lower left portion. Figure 4a is the post-processed conventional RTM. Figure 4b is the inverse scattering RTM. Figure 4c is the velocity model. Note that the steep-dip real event is filtered out from the post-processed conventional RTM while that same event is clearly preserved on the inverse scattering RTM.

Figure 5 compares the conventional RTM and the inverse scattering RTM images of Mississippi Canyon, Gulf of Mexico. A total of 1299 supershots of WAZ data was Tilted Transverse Isotropic (TTI) RTM migrated using a 20-node GPU cluster installed with four M2070 GPU's per node. Figure 5a is the post-processed conventional RTM image. The post-processing includes a low cut wavenumber filtering with cutoff wavenumbers of $k_1 = 0.04k_{max}$, and $k_2 = 0.08k_{max}$, respectively, and a 700 m AGC. Figure 5b is the post-processed inverse scattering RTM image. The post-processing includes a low cut wavenumber filtering with cutoff wavenumbers of $k_1 = 0.01k_{max}$, and $k_2 = 0.02k_{max}$, respectively, and a 1000 m AGC. There are two salt bodies. They are more clear in the inverse scattering RTM image than in the conventional RTM image. The computing time of the inverse scattering RTM is approximately 10% longer than that of the conventional RTM. The longer computing is due to the more complicated imaging algorithm.

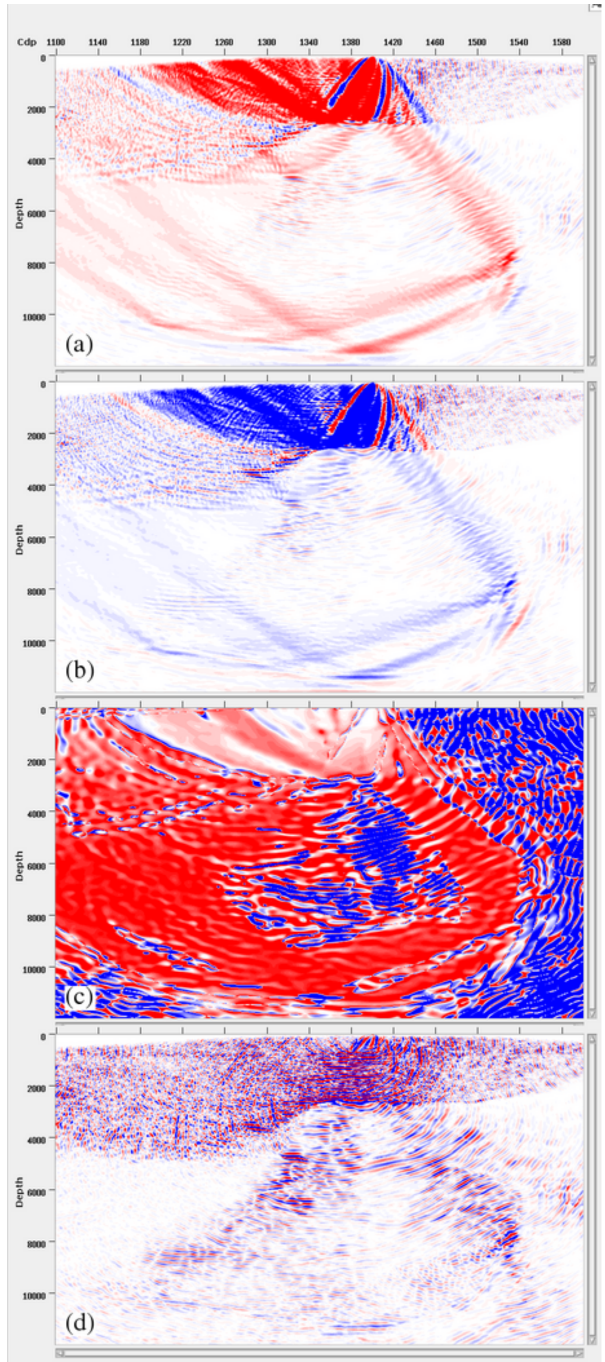

Figure 1: Inverse scattering imaging of one shot. (a) gradient, (b) time derivative, (c) weighting coefficient, and (d) weighted sum of (a) and (b).

DOI http://dx.doi.org/10.1190/segam2013-0686.1

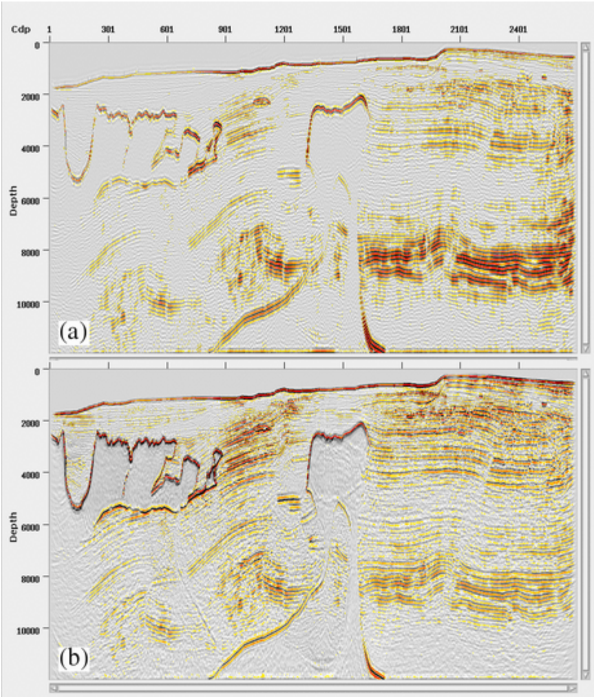

Figure 2: Comparison of conventional RTM and inverse scattering RTM. (a) conventional RTM, and (b) inverse scattering RTM.

DISCUSSION

One of the major issues of RTM is the handling of the source wavefield. This is because the RTM imaging condition requires that the source wavefield (computed via a forward recursion) and the receiver wavefield (computed via a backward recursion) must be available at the same time in an implementation of the algorithm (corss-correlation). The most obvious method is saving all source wavefields on disk memory and retrieving the data as needed. However, this requires huge disk space and i/o time. Another method is reconstructing the source wavefield using the checkpoint method (Symes, 2007; Dussaud et al., 2008) or random boundary method (Clapp, 2009). The source wavefield reconstruction method uses less (or no) disk space but requires more computations.

Our technique uses the first method, i.e., saving the source wavefield snapshot at all cross-correlation times eliminating the source wavefield reconstruction process. Our cross-correlation time interval is decided by the minimum source period (maximum source frequency). Experience shows that four cross-correlations per minimum source wavelet period is sufficient to produce a reasonable RTM image. Also, the wavefield is compressed using a quantization process (float to integer conversion) and a symbolic compression technique such as Hoffman algorithm which achives compression ratio of 10 or more. The CPU is responsible for the compression and disk i/o while the GPU is responsible for the wavefield propagation. If the CPU snapshot time is less than the GPU wave propagation time, the direct wavefield saving method wins. And this is the case for

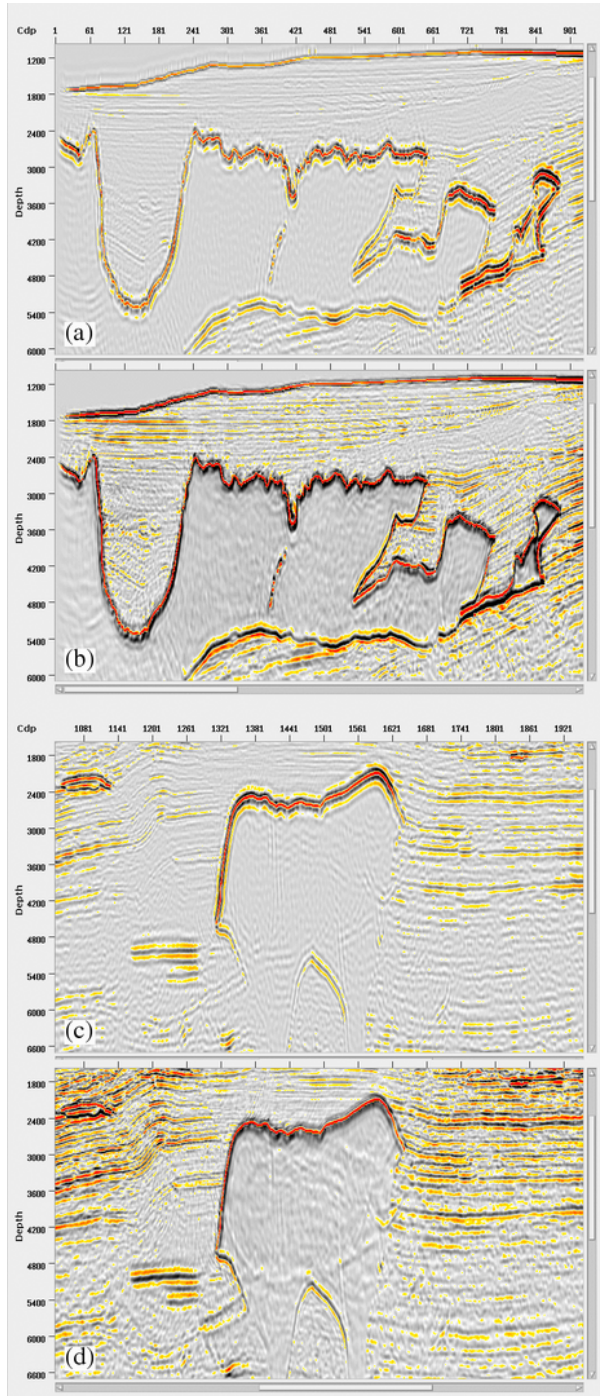

Figure 3: Enlarged comparison of salt bodies. (a) and (b) left salt body, and (c) and (d) right salt body.

DOI http://dx.doi.org/10.1190/segam2013-0686.1

our conventional RTM implementation.

Inverse scattering RTM requires two cross-correlations, i.e., it has to create a gradient image and a time derivative image. We could have computed the time derivative using already saved snapshots. However, it is expensive and inaccurate. Therefore, we compute the time derivative wavefield during the wave propagation and save it as a separate snapshot volume. This strategey resulted in doubling the amount of data to be compressed and written to disk. Because of this, the CPU snapshot time is slightly longer than the GPU wave propagation time in our inverse scattering RTM. To reduce this time delay, we moved a part of the compression process (such as quantization preconditioning) to faster GPU. With this implementation, we were able to reduce the inverse scattering RTM overhead time within 10% compared to that of the conventional RTM time.

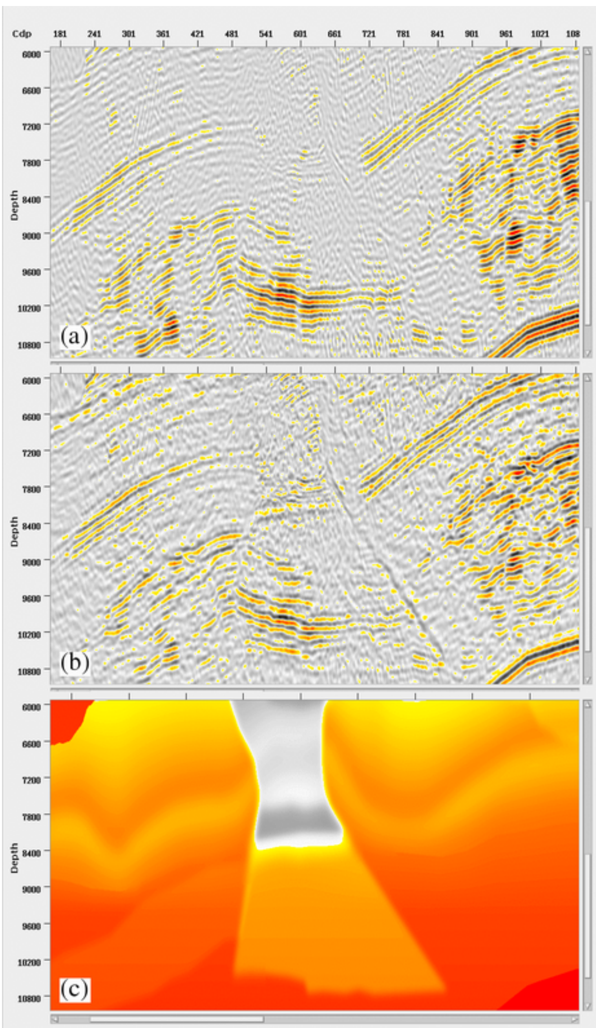

Figure 4: Enlarged comparison of bottom of the left salt. (a) conventional RTM, (b) inverse scattering RTM, (c) velocity model.

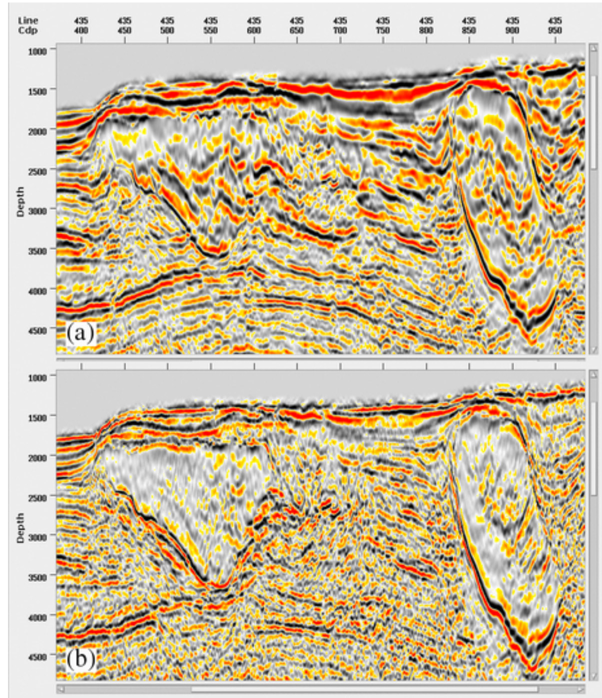

Figure 5: RTM and inverse scattering RTM of Gulf of Mexico data, (a) conventional RTM, (b) inverse scattering RTM.

CONCLUSION

Reverse time migration suffers from low wavenumber noise especially above strong reflectors such as salt boundaries. The traditional method of removing the noise is applying the low cut filtering, which could destroy real events. The inverse scattering imaging condition selectively removes the backscattering noise. We introduce a method of computing an inverse scattering weighting coefficient. The weighting coefficient is computed from the low pass filtered version of the gradient and time derivative images. Synthetic and field examples show that the inverse scattering imaging improves salt boundaries compared to post-processed conventional RTM.

The complicated imaging algorithm requires more computing time. The main overhead comes from the increased amount of source wavefield data. By redistributing some of the data compression process to GPU's, we were able to reduce the run time overhead by 10% of the conventional RTM.

ACKNOWLEDGEMENTS

We thank BP for providing 2004 synthetic data. We thank Laurie Geiger for proof-reading this paper. We thank TGS for permission to publish this paper.

http://dx.doi.org/10.1190/segam2013-0686.1

EDITED REFERENCES

Note: This reference list is a copy-edited version of the reference list submitted by the author. Reference lists for the 2013 SEG Technical Program Expanded Abstracts have been copy edited so that references provided with the online metadata for each paper will achieve a high degree of linking to cited sources that appear on the Web.

REFERENCES

Chang, W. F., and G. A. McMechan, 1986, Reverse-time migration of offset vertical seismic profiling data using the excitation-time imaging condition: Geophysics, **51**, 67–84, http://dx.doi.org/10.1190/1.1442041.

Chang, W. F., and G. A. McMechan, 1990, 3D acoustic prestack reverse-time migration: Geophysical Prospecting, **38**, 737–755, http://dx.doi.org/10.1111/j.1365-2478.1990.tb01872.x.

Claerbout, J. F., 1971, Toward a unified theory of reflector mapping: Geophysics, **36**, 467–481, http://dx.doi.org/10.1190/1.1440185.

Fletcher, B. B., P. J. Fowler, P. Kitchenside, and U. Albertin, 2006, Suppressing unwanted internal reflections in prestack reverse-time migration: Geophysics, **71**, no. 6, E79–E82, http://dx.doi.org/10.1190/1.2356319.

Liu, F., G. Zhang, S. A. Morton, and J. P. Leveille, 2007, Reverse-time migration using one-way wavefield imaging condition: 77th Annual International Meeting, SEG, Expanded Abstracts, 2170–2174, http://dx.doi.org/10.1190/1.2792917.

Mulder, W., and R. Plessix, 2003, One-way and two-way wave-equation migration: 73rd Annual International, Meeting, SEG, Expanded Abstracts, 881–884, http://dx.doi. org/10.1190/1.1818081.

Suh, S. Y., and J. Cai, 2009, Reverse-time migration by fan filtering plus wavefield decomposition: 79th Annual International Meeting, SEG, Expanded Abstracts, 2804–2808, http://dx.doi.org/10.1190/1.3255431.

Whitmore, N. D., and Sean Crawley, 2012, Applications of RTM inverse scattering imaging conditions: 82nd Annual International Meeting, SEG, Expanded Abstracts, http://dx.doi.org/10.1190/segam2012-0779.1.

Yan, R., and X. Xie, 2009, A new angle-domain imaging condition for prestack reverse-time migration: 79th Annual International Meeting, SEG, Expanded Abstracts, 2784–2788, http://dx.doi.org/10.1190/1.3255427.

Yoon, K., and K. J. Marfurt, 2006, Reverse-time migration using the pointing vector: Exploration Geophysics, **37**, 102–107, http://dx.doi.org/10.1071/EG06102.